Structure

Stalking Type III Effector Function

Structure, Vol. 12, 1669–1681, September, 2004, ©2004 Elsevier Ltd. All rights reserved. DOI 10.1016/j.str.2004.06.023

# Crystal Structures of the Type III Effector Protein AvrPphF and Its Chaperone Reveal Residues Required for Plant Pathogenesis

**Alex U. Singer,[1,8] Darrell Desveaux,[2,8] Laurie Betts,[1] Jeff H. Chang,[2] Zachary Nimchuk,[2] Sarah R. Grant,[2,6] Jeffery L. Dangl,[2,3,6,7,*] and John Sondek[1,4,5,*]**

[1]Department of Pharmacology
[2]Department of Biology
[3]Department of Microbiology and Immunology
[4]Department of Biochemistry and Biophysics
[5]Lineberger Comprehensive Cancer Center
[6]Curriculum in Genetics
[7]Carolina Center for Genome Sciences
University of North Carolina at Chapel Hill
Chapel Hill, North Carolina 27599

## Summary

**The *avrPphF* locus from *Pseudomonas syringae* pv. *phaseolicola*, the causative agent of bean halo-blight disease, encodes proteins which either enhance virulence on susceptible hosts or elicit defense responses on hosts carrying the *R1* resistance gene. Here we present the crystal structures of the two proteins from the *avrPphF* operon. The structure of AvrPphF ORF1 is strikingly reminiscent of type III chaperones from bacterial pathogens of animals, indicating structural conservation of these specialized chaperones, despite high sequence divergence. The AvrPphF ORF2 effector adopts a novel "mushroom"-like structure containing "head" and "stalk" subdomains. The head subdomain possesses limited structural homology to the catalytic domain of bacterial ADP-ribosyltransferases (ADP-RTs), though no ADP-RT activity was detected for AvrPphF ORF2 in standard assays. Nonetheless, this structural similarity identified two clusters of conserved surface-exposed residues important for both virulence mediated by AvrPphF ORF2 and recognition of this effector by bean plants expressing the *R1* resistance gene.**

## Introduction

Many Gram-negative bacterial pathogens of either plants or animals use an evolutionarily conserved type III secretion system (TTSS) to deliver proteins, termed type III effectors, directly into host cells. Efficient secretion of a subset of type III effectors requires type III chaperones, which are small acidic proteins that typically bind to a single effector transcribed from the same operon (Parsot et al., 2003). Once inside the host cell, a number of these type III effectors manipulate signaling pathways in order to inhibit host defense mechanisms and aid pathogen colonization (Jin et al., 2003; Staskawicz et al., 2001). Recent findings suggest that the plant immune system, governed by plant disease resistance (*R*) genes, recognizes the virulence activity of type III effectors (Axtell and Staskawicz, 2003; Mackey et al., 2002, 2003; Shao et al., 2003). These observations support a general model in which indirect recognition of the action of pathogen virulence factors initiates successful plant immune responses (Dangl and Jones, 2001; Van der Biezen and Jones, 1998; Van der Hoorn et al., 2002).

Functions for some type III effectors from animal pathogens have been described. For example, the extracellular mammalian pathogen *Yersinia* injects at least six type III effectors into cells, four of which are enzymes that inhibit cytoskeletal dynamics to prevent phagocytosis: YopH is a highly potent tyrosine phosphatase; YopE functions as a Rho-GAP (GTPase activating protein); YopT is a cysteine protease that targets Rho family GTPases; and YopO/YpkA is a Ser/Thr kinase (Cornelis, 2002). Similarly, the intracellular pathogen *Salmonella* delivers two sets of type III effectors during distinct phases of its infection cycle (Galan, 2001; Hansen-Wester and Hensel, 2001). The first set is required to reprogram eukaryotic actin to allow endocytosis of *Salmonella*, while the second set prevents endocytic vacuoles from fusing with lysosomal vacuoles, thereby facilitating retrograde bacterial transport.

In contrast, functions for type III effectors from plant pathogens remain poorly characterized. Recent genome-wide analyses for proteins that might be substrates for the type III secretion system of the plant pathogen *Pseudomonas syringae* pathovar *tomato* (*Pst*) DC3000 revealed ~50 confirmed or predicted type III effectors (Boch et al., 2002; Collmer et al., 2002; Fouts et al., 2002; Greenberg and Vinatzer, 2003; Guttman et al., 2002; Petnicki-Ocwieja et al., 2002; Zwiesler-Vollick et al., 2002). Furthermore, several type III effectors of *P. syringae* increase virulence on genetically susceptible hosts (Chang et al., 2000; Chen et al., 2000; Lorang and Keen, 1995; Nimchuk et al., 2001; Ritter and Dangl, 1995). However, despite increasing efforts, biochemical functions have been assigned to a paltry few *P. syringae* type III effectors (Axtell et al., 2003; Espinosa et al., 2003; Shao et al., 2002). Consequently, understanding the function of type III effector proteins in virulence and in triggering host disease resistance is currently a major goal in the study of plant pathology.

In response to this dearth of functional data and the mounting realization that conventional biochemical and genetic techniques do not readily yield functional assignments for type III effectors, we initiated a structural approach to further characterize *P. syringae* type III effectors in order to gain insight into their mechanisms of action. Here, we present the crystal structures of the two gene products (ORF1 and ORF2) of the *avrPphF* locus. This locus resides in a pathogenicity island on the naturally occurring plasmid pAV511 of the bean pathogen *P. syringae* pv. *phaseolicola* (Jackson et al., 1999; Tsiamis et al., 2000). AvrPphF ORF1 and ORF2 are both required for maximal virulence of *P. syringae* on susceptible plants, as well as for the initiation of specific host immune responses on genetically resistant

*Correspondence: dangl@email.unc.edu (J.L.D.); sondek@med.unc.edu (J.S.)
[8]These authors contributed equally to this work.

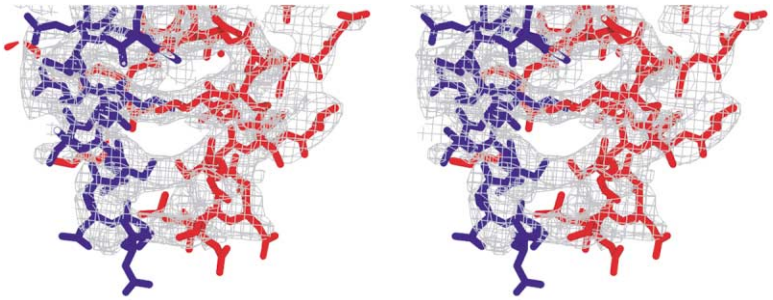

Figure 1. Stereoview of Experimental Electron Density for AvrPphF ORF1

The region highlighted is along the dimer interface mediated by α2 helices, and the two participating monomers are colored blue and red for clarity. The map shown is contoured at 0.8 σ using phases derived from multiple anomolous wavelength data at 3.0 Å resolution.

plants (Tsiamis et al., 2000). More specifically, on susceptible bean cultivars (inbred strains) that lack the *R1* resistance gene, such as Tendergreen, AvrPphF enhances pathogen growth and is thus a virulence factor. Conversely, on cultivars possessing the *R1* resistance gene, such as Red Mexican, AvrPphF is recognized by the plant immune system and is therefore experimentally defined as an avirulence factor.

The crystal structure of AvrPphF ORF1 confirms its predicted role as a type III chaperone; in contrast, the structure of AvrPphF ORF2 is novel. The structure of AvrPphF ORF2 was used to identify surface residues required for both the virulence and avirulence functions of AvrPphF. These results validate a structure-based effort to identify key functional features of *P. syringae* type III effectors and highlight the importance of structural analyses to complement biochemical and genetic techniques in order to maximize the deduction of functional information.

## Results

### The AvrPphF ORF1 Structure Indicates Universality among Type III Effector Chaperones

The crystal structure of AvrPphF ORF1 was determined to a resolution of 3 Å using multiwavelength anomalous dispersion (Figures 1 and 2; Table 1). There are four molecules per asymmetric unit. However, one dimer interface mediated by a central pair of symmetrical helices (α2) predominates (total buried surface area of 3548 Å$^2$) and resembles the extensive dimer interface found in structures of other type III chaperones (Parsot et al., 2003). Therefore, it is most likely that this dimeric form of AvrPphF ORF1 is the biologically relevant unit. This interpretation is supported by the fact that AvrPphF ORF1 is dimeric in solution based upon gel exclusion chromatography (data not shown). Like other dimeric type III chaperones, the α2 helix of AvrPphF ORF1 predominantly contributes intermolecular interactions within the dimer (Figure 1). Centered within the dimeric interface, Cys67 of the α2 helix forms an intermolecular disulfide bond. However, this cysteine is not conserved among alleles of AvrPphF ORF1 and most likely is not critical for maintaining the dimeric form of AvrPphF ORF1 (Figure 2C).

Structural comparisons using the program DALI (Holm and Sander, 1993) report highly significant Z scores of ~10–12 between AvrPphF ORF1 and other type III chaperones, including *Yersinia pseudotuberculosis* SycE (PDB code: 1JYA [Birtalan and Ghosh, 2001; Birtalan et al., 2002]), *Salmonella typhimurium* SicP (PDB code: 1JYO [Stebbins and Galan, 2001]), enterohemorrhagic *E. coli* CesT (PDB code: 1K3E [Luo et al., 2001]), and *Salmonella enterica* SigE (PDB code: 1K3S [Luo et al., 2001]), despite low sequence similarity (% identity between AvrPphF ORF1 and these four chaperones varies from ~15% for SicE and SigE to 8% for SicP and CesT). Like other type III chaperones, AvrPphF ORF1 adopts an α-β-β-β-α-β-β-α topology with a significant negatively charged electrostatic surface and two pairs of hydrophobic patches. In particular, the fold of SycE, the chaperone of the *Yersinia* effector YopE, is virtually identical to that of AvrPphF ORF1 (Figure 2A). One hundred and six Cα residues of AvrPphF ORF1 and SycE can be superimposed with a root-mean-square deviation (rmsd) of 2.5 Å calculated using the DALI server (Holm and Sander, 1993). The structural similarity between AvrPphF ORF1 and other type III chaperones suggests the preservation of common functions through structural conservation.

Currently, there are no published cocrystal structures of a type III chaperone with a full-length effector. However, there are two crystal structures of type III chaperones bound to N-terminal fragments of their cognate type III effectors. These are the structures of SicP bound to its effector SptP (Stebbins and Galan, 2001) and SycE in complex with its cognate effector YopE (Birtalan et al., 2002). The SicP/SptP and SycE/YopE interactions are mediated predominantly by hydrophobic interactions located at two distinct patches on the chaperone homodimer surface (Figure 2B). The first patch lies in a concavity that accommodates an α helix of the respective effector (helix binding groove, or patch 1), while the second hydrophobic patch binds to a β strand of the effector (patch 2) (Stebbins and Galan, 2001; Birtalan et al., 2002) (see Figure 2B). The surface of the AvrPphF ORF1 dimer displays similar regions; however, the chemical nature of these patches is not as highly hydrophobic as SycE and SicP. Interestingly, there are two distinct hydrophobic patches on the AvrPphF ORF1 homodimer surface. The first hydrophobic patch is located near one end of the aforementioned putative helix binding grooves and along the dimer interface, and includes a shallow depression containing the residues Pro83, Phe84, and Phe85 (Figure 2B), which are well conserved among AvrPphF ORF1 alleles (Figure 2C). The second hydrophobic patch of AvrPphF ORF1 (patch 2) is formed by conserved residues Phe7, Pro21, Phe23, Tyr33, and Phe5 and is adjacent to the helix binding groove (Figures 2B and 2C). Therefore, if the interaction of AvrPphF ORF1 and ORF2 is mediated by mainly hydrophobic interactions, the location of candidate surfaces on the

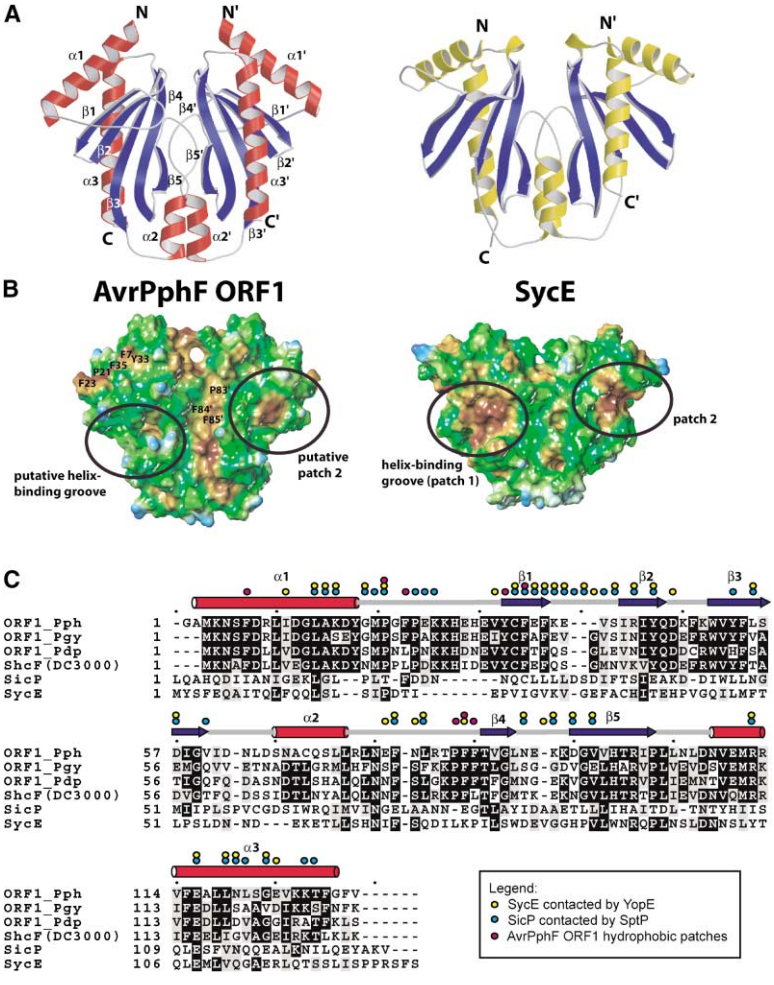


Figure 2. Structural Similarity between AvrPphF ORF1 and *Yersinia pseudotuberculosis* SycE

(A) Ribbon diagrams emphasize the structural similarity of AvrPphF ORF1 (left) to the chaperone SycE (right; PDB code: 1L2W [Birtalan et al., 2002]). The major helices (α1–α3) of each monomer are colored to emphasize their similar tertiary and quaternary structures.

(B) AvrPphF ORF1 shares surfaces features with SycE required for binding type III effectors. MOLCAD surfaces of AvrPphF ORF1 and SycE were generated using the program SYBYL version 6.9.1 (www.tripos.com) and were colored by hydrophobic potential (Ghose et al., 1998; Viswandam et al., 1989) over a range of −0.25–0.05, where blue to green to brown represents the spectrum from hydrophilic to hydrophobic regions. The two hydrophobic effector binding regions on SycE (Birtalan and Ghosh, 2001; Birtalan et al., 2002) are circled and labeled, as are the corresponding surfaces on AvrPphF ORF1. Note that patches one and two arise from molecules 1 and 2 of the dimer, respectively, and that a rotation of 180° about the vertical would result in display of the same surfaces but on opposite molecules. Additional conserved residues on two additional hydrophobic regions on the AvrPphF ORF1 surface are also labeled.

(C) Multiple sequence alignment of AvrPphF ORF1 alleles with SicP and SycE. Alignment of the four AvrPphF ORF1 alleles was performed with ClustalX (Jeanmougin et al., 1998), while alignment of AvrPphF ORF1 from *P. syringae* pv. *phaseolicola* (ORF1_Pph) with SicP and SycE was done using the structural alignment output from DALI. Positions of helices (red cylinders) and β strands (blue arrows) in the AvrPphF ORF1 structure are shown. Chaperone residues with buried surface areas of >10 Å$^2$ due to effector binding in the SicP/SptP or SycE/YopE complexes are highlighted with blue or yellow circles, respectively, while residues of AvrPphF ORF1 associated with the additional hydrophobic surfaces in Figure 2B are highlighted with magenta circles. Buried surface area was calculated using the program NACCESS (Hubbard and Thornton, 1993). Sequences used in the alignment are from *P. syringae* pv. *phaseolicola* (ORF1_Pph), *P. syringae* pv. *glycinea* (ORF1_Pgy [J.H.C., unpublished data]), *P syringae* pv. *delphinii* (ORF1_Pdp, GenBank accession number AAP23119.1), *P. syringae* pv. *tomato* strain DC3000 (ORF1_DC3000, AA054047.1), *Yersinia pseudotuberculosis* SycE (1L2W), and *Salmonella typhimurium* SicP (1JYO).

ORF1 dimer suggests a different mode of interaction than that observed for SicP/SptP and SycE/YopE.

In addition, we note the conservation of Glu116 among AvrPphF ORF1 alleles, which in SicP and SycE forms a salt bridge with a conserved arginine in the corresponding virulence factors. This observation supports conservation of some specificity in chaperone/effector interactions.

### The Structure of AvrPphF ORF2 Is Novel

The structure of AvrPphF ORF2 (Figure 3; Table 1) was determined by multiple isomorphous replacement with anomalous scattering using crystals soaked in high concentrations of CsCl (Dauter et al., 2000, 2001). AvrPphF ORF2 forms an elongated structure (~60 Å × 20–35 Å) somewhat reminiscent of a mushroom that can be divided into "stalk" and "head" subdomains (Figures 3 and 4). The stalk subdomain is composed of the N-terminal helix (α1) and β strands β3-β4. An antiparallel β sheet (β5, β7-β8) forms the base of the head subdomain that interacts with the stalk. A pair of twisted antiparallel β sheets (β1 and β6; β2 and β9/9′) supported by α2 form the dome of the head.

Alleles of AvrPphF ORF2 have no significant sequence similarity to other proteins (data not shown). However, the head subdomain of AvrPphF ORF2 possesses weak structural similarity with the catalytic portion of a number of ADP-ribosyltransferase (ADP-RT) toxins (Figure 4). For example, structural comparisons using the DALI server indicate the strongest structural similarity (Z score = 4.3 over 79 Cα atoms, rmsd of 2.9 Å, 10% sequence identity) between the head subdomain and the catalytic domain of diphtheria toxin (PDB code: 1DDT [Bennett et al., 1994]) (Figures 4C and 4D). Specifically, AvrPphF ORF2 strands β1, β5, β6, β7, β8, and β9′ superimpose in whole or in part with diphtheria strands CB2, CB3, CB4, CB6, CB7, and CB8, respectively (using the nomenclature of Bennett et al. [1994]) (Figure 4D). Despite this structural relatedness, AvrPphF ORF2 did not possess NAD glycohydrolase activity using an in vitro fluorescence assay which monitors the increase in quantum yield that occurs when etheno-NAD (Sigma-

Table 1. Data Collection and Refinement Statistics

| Structure | AvrPphF ORF1 | | | AvrPphF ORF2 | |
|---|---|---|---|---|---|
| Data set | λ1 | λ2 | λ3 | Native | CsCl |
| **Data Collection** | | | | | |
| Wavelength (Å) | 0.97925 | 0.97936 | 0.97167 | 1.5418 | 1.5418 |
| Resolution (Å) | 20.0–3.0 | 20.0–3.0 | 20.0–3.1 | 20.0–2.0 | 20.0–2.4 |
| Total observations | 139,782 | 140,056 | 140,110 | 58,578 | 118,527 |
| Unique reflections | 18,973 | 19,032 | 19,032 | 16,442 | 9,639 |
| Completeness (%) | 100.0 (100.0)[a] | 100.0 (100.0) | 100.0 (100.0) | 99.8 (99.1) | 99.9 (98.7) |
| $I/\sigma$[b] | 26.9 (7.7) | 23.8 (4.8) | 20.5 (3.4) | 18.9 (6.1) | 29.0 (4.5) |
| $R_{sym}$[c] | 9.6 (25.7) | 9.6 (44.5) | 10.3 (63.0) | 5.4 (23.3) | 10.6 (30.9) |
| **Refinement and Model Statistics** | | | | | |
| Resolution (Å) | 20–3.0 | | | 20–2.0 | |
| Mean figure of merit[d] | 0.628/0.776 | | | 0.425/0.796 | |
| Reflections (working/test) | 17,577/893 | | | 15,610/798 | |
| $R_{work}$[e] (%) | 24.1 | | | 22.5 | |
| $R_{free}$[f] (%) | 28.9 | | | 24.1 | |
| Mean B factor (overall, Å$^2$) | 44.1 | | | 33.6 | |
| Wilson B factor (Å$^2$) | 72.4 | | | 18.6 | |
| Rms deviations | | | | | |
| Bond lengths (Å) | 0.009 | | | 0.005 | |
| Bond angles (°) | 1.4 | | | 1.3 | |
| Ramachandran plot | | | | | |
| % in most favored regions | 80.6 | | | 88.5 | |
| % in additional allowed regions | 17.7 | | | 11.5 | |
| % in disallowed regions | 0.0 | | | 0.0 | |

[a] Values in parentheses refer to the highest resolution shell.
[b] $I/\sigma$ = mean signal to noise, where I is the integrated intensity of a measured reflection, and $\sigma$ is the estimated error in measurement.
[c] $R_{sym} = 100 \times \Sigma|1 - <I>/\Sigma I$, where I is the integrated intensity of each measured reflection.
[d] For AvrPphF ORF1 phase determination, these represent FOM values before and after solvent flattening with DM (CCP4, 1994), both at 3 Å. For AvrPphF ORF2, these FOM values represent phases to 2.4 Å before and after using the solvent-flattening routine in SHELXE (Schneider and Sheldrick, 2002).
[e] $R_{work}=\Sigma|F_o - F_c|/\Sigma F_o$, where $F_o$ and $F_c$ are defined as the observed and calculated structure factor amplitudes.
[f] $R_{free}$ is calculated as defined by $R_{work}$ using test set reflections (5% of the total).

Aldrich) is hydrolyzed (Beattie and Merrill, 1999). Similarly, purified AvrPphF ORF2 had no ADP-RT activity in an assay that examined labeling of proteins in an *Arabidopsis* cell extract containing radiolabeled NAD (Coburn et al., 1989), even if supplemented with its cognate chaperone AvrPphF ORF1 (data not shown). However, both activities were readily demonstrated with the catalytic domain of exotoxin A of *Pseudomonas aeruginosa*, a known ADP-RT (Iglewski and Kabat, 1975). Similarly, crystals of AvrPphF ORF2 either grown with NAD (10 mM) or soaked with similar concentrations of NAD prior to data collection showed no electron density consistent with bound NAD. Manually docking of NAD into the putative active site of AvrPphF ORF2 suggests that a β strand (β2), with no equivalent in diphtheria toxin, sterically blocks binding of NAD.

### Structure-Based Identification of Key Functional Residues in AvrPphF ORF2

Structural conservation of catalytic residues between different enzymes has been described (e.g., for transglutaminases and cysteine proteases [Makarova et al., 1999]). Therefore, despite the lack of AvrPphF ORF2 ADP-RT activity, we used the structural homology to diphtheria toxin and amino acid conservation across multiple alleles of AvrPphF ORF2 as predictors of residues required for function.

For instance, in diphtheria toxin, amino acids His21 and Glu148 correspond to critical catalytic residues required for ADP-RT activity (Takada et al., 1995). In ADP-RTs, His21 corresponds to a conserved basic residue which hydrogen bonds to the adenosine ribose, while Glu148 corresponds to an absolutely conserved catalytic residue which extracts a proton from the 2′ hydroxyl of the nicotinamide-linked ribose. In AvrPphF ORF2, Arg72 and Asp174 are spatially equivalent to His21 and Glu148, respectively, from diphtheria toxin (Figures 4A and 4C). This suggests a potential for these residues in mediating the virulence activity of AvrPphF ORF2. We additionally identified residues conserved between alleles of AvrPphF ORF2 that lie on exposed surfaces of the molecule. Two surface regions on opposing sides of the molecule harbor residues conserved between the four AvrPphF ORF2 alleles (Figure 5). The first surface encompasses the region that shares structural homology to the NAD binding site of ADP-RT toxins and forms

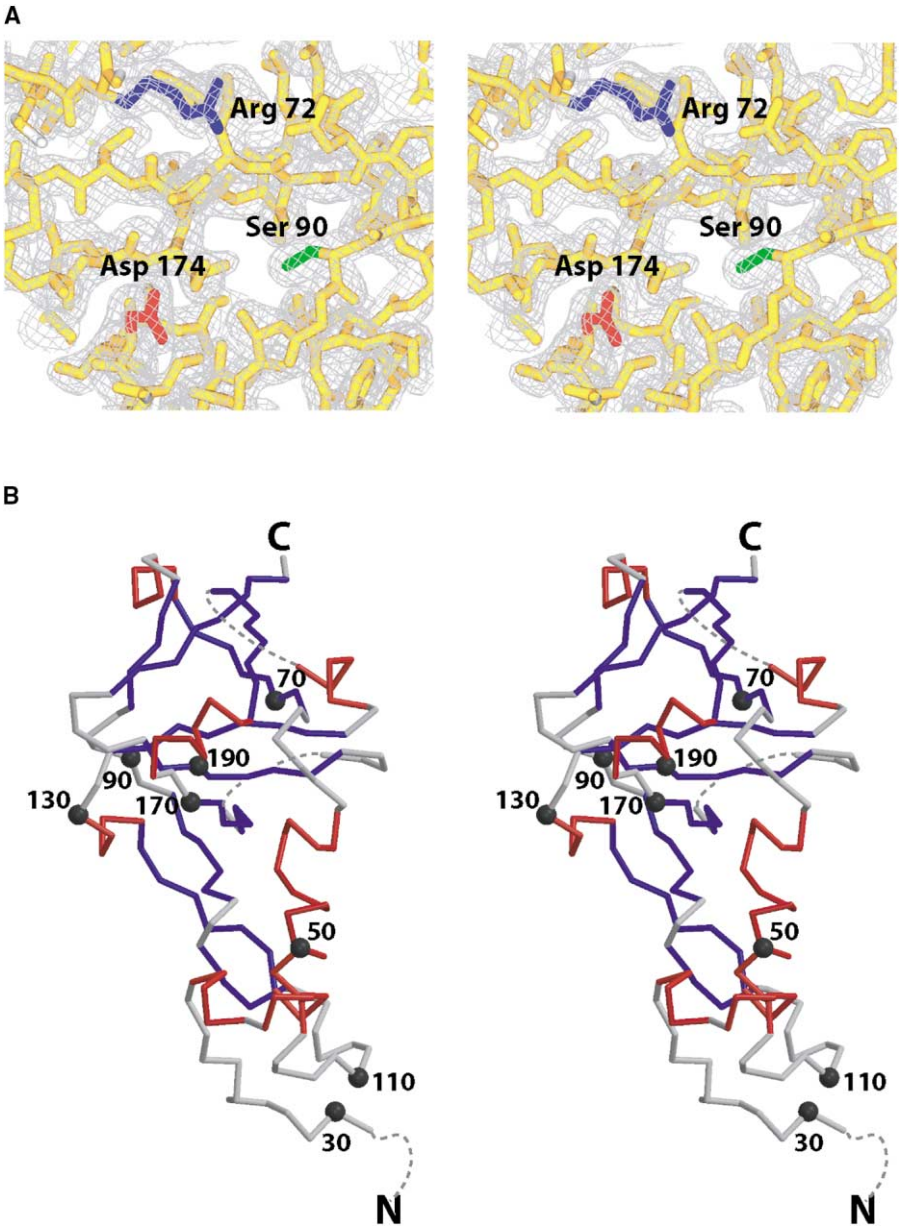


Figure 3. The Structure of the AvrPphF ORF2 Type III Effector Is Novel

(A) Stereoview of experimental electron density for AvrPphF ORF2 derived from MIRAS phases. The displayed region (pocket A, see text) contains a large number of conserved residues among alleles of AvrPphF ORF2 including Arg72 (blue), Ser90 (green), and Asp174 (red) chosen for site-directed mutagenesis. The experimental electron density map is contoured at 1.0 $\sigma$ at 2.0 Å resolution.

(B) Stereoview of the backbone trace of AvrPphF ORF2. Beginning at residue 30, every 20th residue is labeled and marked with a black sphere, helices are red, and $\beta$ strands are blue. Disordered regions are indicated with dotted lines.

a groove in the head subdomain. We termed this "pocket A." Pocket A possesses fourteen residues that are absolutely conserved between AvrPphF ORF2 alleles including the exposed Arg72 and Asp174. On the opposite side of the protein, a second conserved surface is located at the interface between the head and stalk (pocket B). Conserved residues on these two surfaces are both hydrophilic and hydrophobic. However, hydrophilic residues were favored for mutagenesis due to their role in hydrogen bonding and the higher probability that they could be involved in catalytic activities. Using these combined criteria, we mutated Ser90 in addition to Arg72 and Asp174 in pocket A and also chose His97 and Glu98 for mutagenesis in pocket B.

Wild-type and mutated versions of AvrPphF ORF2 were fused to a C-terminal HA-epitope tag, cloned into the expression vector pDSK600 (Keen et al., 1988), and transformed into the RW60 strain of *P. syringae* pv. *phaseolicola* (*Pph*). *Pph* RW60 is cured of the pAV511 plasmid that normally harbors the *avrPphF* ORF1 and

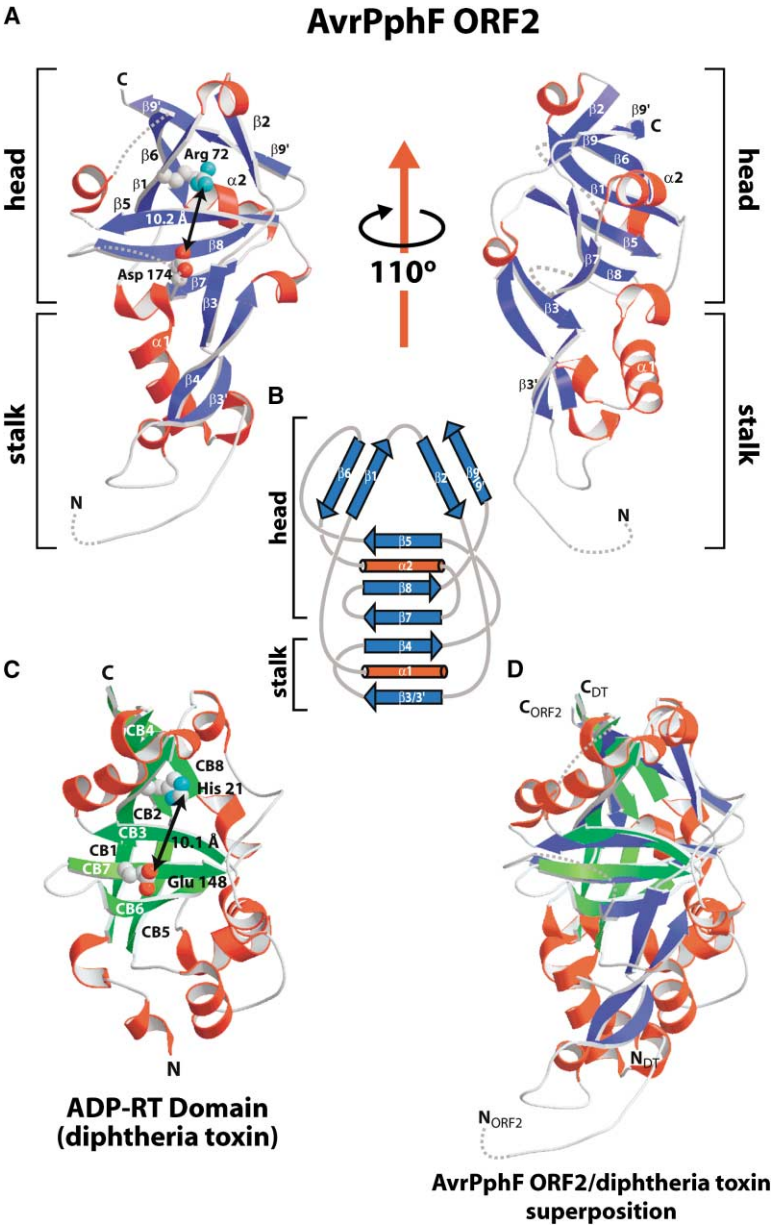


Figure 4. Structural Similarity between AvrPphF ORF2 and an ADP-Ribosyltransferase

(A) Ribbon trace of AvrPphF ORF2 in two orientations related by 110° and emphasizing the stalk and head subdomains. Of the helical segments (red), only two (helices αA and αB) extend for more than one turn and have been noted. β strands are blue and dashed lines represent disordered regions at the N terminus, residues 147–153, and residues 177–180.

(B) Topological diagram of the AvrPphF ORF2 fold highlighting the three sets of β strands (β1and β6; β2 and β9,9′; β5, β7, and β8) approximately arranged in mutually supporting triangles and composing the majority of the head subdomain.

(C) Structural similarity of AvrPphF ORF2 and diphtheria toxin. Shown is a ribbon diagram of the ADP-ribosyltransferase domain of diphtheria toxin highlighting the critical catalytic residues, His21 and Glu148. The functionally similar Arg72 and Asp174 are located at equivalent positions in the AvrPphF ORF2 structure (upper left panel in [A]). The distance between the residues on both structures is indicated in Å. Strands are labeled according to the nomenclature of Bennett et al. (1994).

(D) Superposition of AvrPphF ORF2 with the catalytic domain of diphtheria toxin. A ribbon diagram of these two structures superimposed using the structurally aligned residues listed from DALI is shown. The orientation of these two molecules is identical to that shown in Figures 3A and 3C. The N- and C termini of each molecule are labeled.

ORF2 operon (Tsiamis et al., 2000). ORF1 was cloned into the vector pBBR1 MCS-2 (Kovach et al., 1995) and also transformed into each strain. Pathogenic growth of these bacteria was monitored on the susceptible Tendergreen bean cultivar. RW60 carrying the empty pDSK600 vector and expressing AvrPphF ORF1 grew approximately 20-fold over 2 days (Figure 6A). The presence of wild-type AvrPphF ORF2 in this strain increased pathogen growth by an additional ~10-fold, reflecting the AvrPphF ORF2 virulence function (Tsiamis et al., 2000). Mutation of either Arg72 (R72A) or Asp174 (D174A) in pocket A eliminated the virulence function of AvrPphF ORF2. Mutation of Ser90 (S90A) did not eliminate the virulence function, though slight losses in virulence were observed in some experiments (data not shown). Last, mutation of His97 (H97A) or Glu98 (E98A) had an intermediate effect, increasing pathogen growth by ~5-fold relative to RW60 carrying an empty vector. Western blot analysis confirmed that each protein was the correct molecular weight and expressed to a similar level (Figure 6C).

Many type III effectors from plant pathogenic bacteria are also the determinants recognized by the plant's immune system (see Introduction). Therefore, we determined if amino acids important for the virulence function of AvrPphF ORF2 are also required for its ability to trigger a specific host disease resistance response. Growth of the *Pph* RW60 strains expressing wild-type and mutant AvrPphF ORF2 proteins was examined on the bean cultivar Red Mexican, which expresses the *R1* disease resistance gene (Figure 6B). Virulent *Pph* RW60 carrying an empty pDSK600 vector and expressing AvrPphF ORF1 grew robustly over 3 days on this cultivar. Expression of wild-type AvrPphF ORF2 significantly reduced

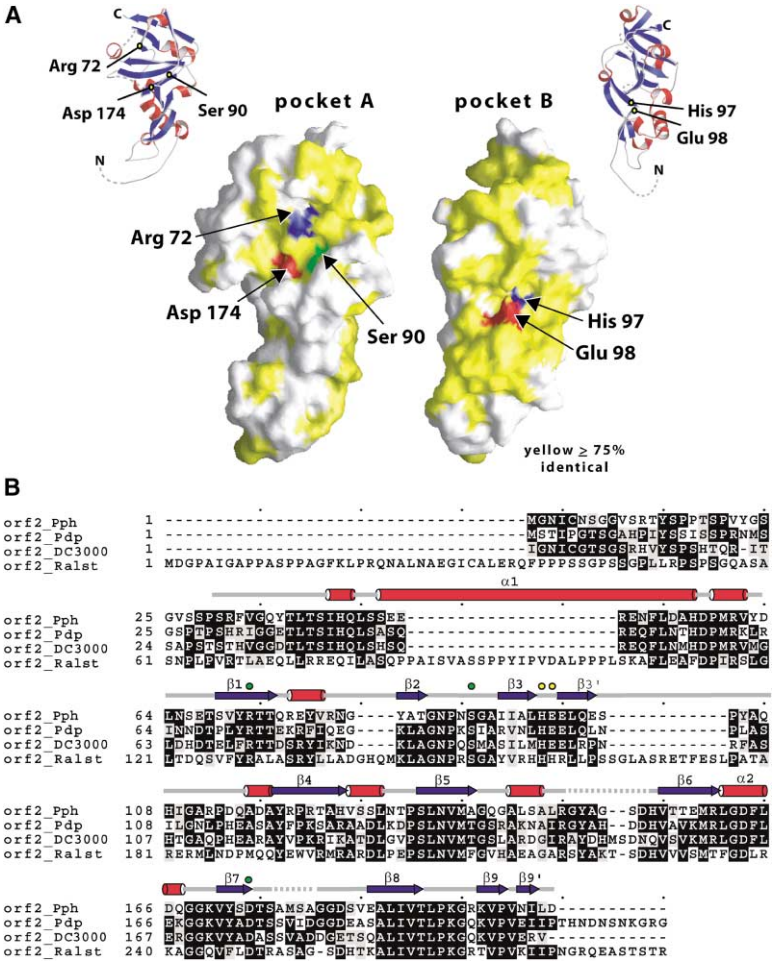


Figure 5. Conserved Surface Residues of AvrPphF ORF2

(A) There are two highly conserved surface patches in alleles of AvrPphF ORF2. Shown are two surface representations of AvrPphF ORF2 related by an ~110° rotation about the vertical axis, with residues identical in at least three of the four AvrPphF alleles highlighted yellow. Enumerated residues are essentially invariant among the alleles and were mutated in this study. The left orientation highlights pocket A, the right orientation highlights pocket B, and the associated ribbon diagrams (insets) indicate the underlying structure for the respective surfaces. Orientations shown in this figure are identical to those in Figure 4.

(B) Amino acid sequence alignment of the four alleles of AvrPphF ORF2. Helical segments (red cylinders) and β strands (blue arrows) in AvrPphF OFR2 are shown. Residues targeted for mutation are highlighted with green (pocket A) and yellow (pocket B) circles. Sequences with associated GenBank accession numbers used in the alignment are from *P. syringae* pv. *phaseolicola* (ORF2_Pph, AAF67149.1), *P. syringae* pv. *delphinii* (ORF2_Pdp, AAP23118.1), *P. syringae* pv. *tomato* strain DC3000 (ORF2_DC3000, AA054046.1), and *Ralstonia solanacearum* (ORF2_Ralst, NP_522383.1).

pathogen growth, reflecting recognition of *Pph* RW60 by the bean *R1* disease resistance gene (Tsiamis et al., 2000). In parallel to our observations of the AvrPphF ORF2 virulence function, the pocket A mutations R72A and D174A abolished the resistance response, S90A did not, and pocket B mutations, H97A and E98A, had an intermediate effect. Therefore, AvrPphF ORF2 amino acids important for its virulence activity are also required for optimal recognition of the presence of this type III effector by the bean *R1* gene product.

To exclude the possibility that mutation of Arg77 or Asp174 eliminated AvrPphF ORF2 functions by disruption of proper protein folding or favoring aggregation, we expressed both mutant proteins in *E. coli*. We found that these proteins were soluble when prepared from *E. coli* cell extracts and that the resulting proteins were monomeric on gel filtration columns (Figure 6D). Furthermore, wild-type and mutant proteins yielded very similar circular dichroism spectra (Figure 6E), indicating the similarity of their folds.

## Discussion

The crystal structures of AvrPphF ORF1 and AvrPphF ORF2 represent the first structures of a type III chaperone and its corresponding type III effector from a plant pathogen. Interestingly, despite low sequence similarity (8%–14%), the structure is very similar to that of chaperones from the animal pathogens *Yersinia*, enteropathogenic *E. coli*, and *Salmonella*, suggesting that chaperones of plant and animal pathogens use similar mechanisms to promote the secretion of type III effectors. The identification of AvrPphF ORF1 as a type III chaperone is not surprising, for two reasons: First, despite low sequence conservation, the protein-threading server 3D-PSSM (Kelley et al., 2000) identified the known type III effectors SycE and SigE as likely structural homologs. Second, the recently sequenced *tomato Pst* DC3000 genome contains homologs of both AvrPphF ORF1 and AvrPphF ORF2 within the same operon. The DC3000 homolog ShcF, which shares ~50% identity in protein sequence to AvrPphF ORF1 (Figure 2C), was designated a type III chaperone for the AvrPphF ORF2 homolog HopPtoF prior to determination of the AvrPphF ORF1 structure and has been recently demonstrated to function as chaperone for HopPtoF in vivo (Shan et al., 2004).

The cocrystal structures of SicP/SptP and SycE/YopE have shown that chaperones bind to regions of type III effectors that contain secondary, but little tertiary, structure and have highlighted the effector wrapping around chaperone dimers (Birtalan et al., 2002; Stebbins and Galan, 2001). From these structures, it has been

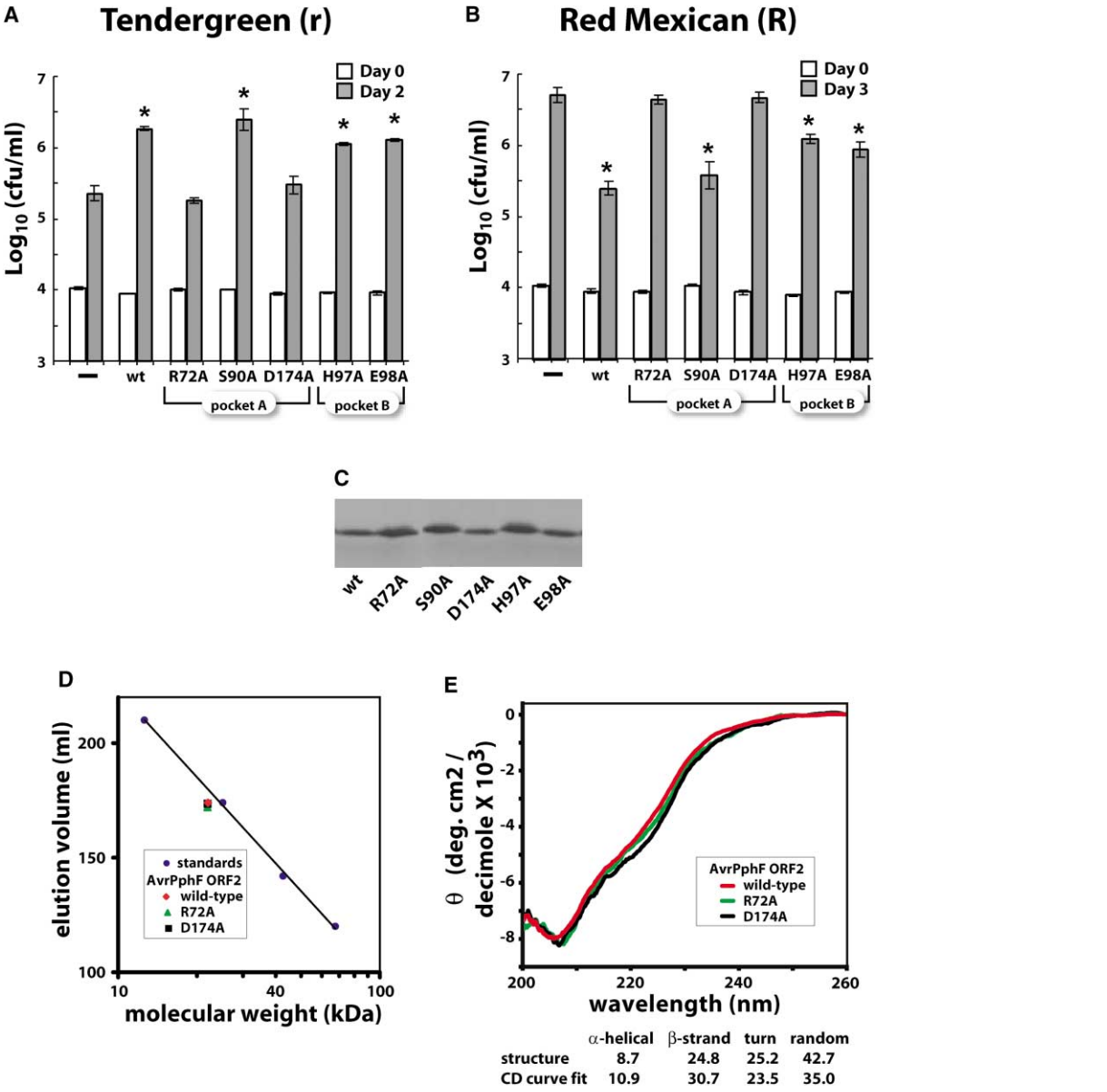


| | α-helical | β-strand | turn | random |
|---|---|---|---|---|
| structure | 8.7 | 24.8 | 25.2 | 42.7 |
| CD curve fit | 10.9 | 30.7 | 23.5 | 35.0 |

Figure 6. Conserved Surface Residues of AvrPphF ORF2 Are Required for Both Virulence and Avirulence Activities

(A) Growth of *P. syringae* pv. *phaseolicola* strain RW60 expressing wild-type and mutant versions of AvrPphF-HA on the Tendergreen bean cultivar, where AvrPphF acts as a virulence factor. White and gray bars represent the bacterial populations immediately post inoculation (day 0) and 2 days post inoculation. (−) represents the negative control strain carrying an empty pDSK600 vector. Error bars represent the standard error of the mean of three samples. Results are representative of four independent experiments. Asterisks indicate values that are significantly different from the empty vector as determined by one-way ANOVA (*$p < 0.05$). All strains also carry a second plasmid expressing avrPphF ORF1.

(B) Growth of *P. syringae* pv. *phaseolicola* strain RW60 expressing the wild-type and mutant versions of AvrPphF-HA on the Red Mexican bean cultivar where AvrPphF acts as an avirulence factor triggering disease resistance via the bean R1 disease resistance gene. White and gray bars represent the bacterial populations immediately post inoculation (day 0) and 3 days post inoculation. Other symbols are described in the previous panel. All strains also carry a second plasmid expressing avrPphF ORF1.

(C) Western blot analysis using anti-HA antibodies of soluble protein from *P. syringae* RW60 expressing the various AvrPphF proteins. 10 μg of soluble protein was loaded in each lane.

(D) Gel filtration of wild-type AvrPphF ORF2 and R72A and D174A mutant proteins. The three proteins migrate with virtually identical mobilities on a Sephacryl S200 column (Pharmacia) with an apparent molecular weight of ~25 kDa based upon the elution of molecular weight standards. In comparison, the calculated molecular weight is ~22 kDa for the wild-type and mutant proteins.

(E) Circular dichroism spectra of wild-type AvrPphF ORF2 and R72A and D174A mutant proteins. Mean molar ellipticity is plotted as a function of wavelength, and the spectra of the wild-type and mutant proteins are found to be virtually identical. The spectrum of the wild-type protein was curve-fit using the program CONTINLL (Provencher and Glockner, 1981) and found to contain a similar component of secondary structural elements as calculated from the coordinates of the structure and listed beneath the spectra.

proposed that chaperones may contribute to effector secretion by maintaining them in partially unfolded, secretion-competent states (Stebbins and Galan, 2001). Alternatively, it has been proposed that the three-dimensional structure of the chaperone/effector complex may provide a translocation signal for secretion (Birtalan et al., 2002). Consistent with either scenario, and unlike other chaperones such as Gro/EL and DnaK/Hsp70 protein families, type III chaperones are not believed to be involved in folding of the effector, since identical Rho-GAP activities are found for YopE alone or in complex with its chaperone SycE (Birtalan et al., 2002). In addition, the *E. coli* effector Tir has an identical affinity for the intimin receptor alone and in complex with its chaperone CesT (Luo et al., 2001). Recently, the *E. coli* chaperone CesT has been demonstrated to interact with the TTSS ATPase component, EscN (Gauthier and Finlay, 2003), indicating that type III chaperones may specifically interact with components of the TTSS apparatus, allowing for efficient transport of the effector to the type III pilus.

AvrPphF ORF1 possesses two hydrophobic patches similar to those that mediate interactions of SycE and SicP with their corresponding effectors (Figure 2B). However, the novel arrangement of these patches on the surface of the ORF1 molecule may indicate a novel mode of chaperone/effector interaction for AvrPphF. Furthermore, type III chaperones bind to an ~60–100 residue region of the effector in a partially unfolded conformation (Birtalan et al., 2002; Stebbins and Galan, 2001). In YopE and SptP, chaperone binding regions lie N-terminal to GAP domains (Evdokimov et al., 2002; Stebbins and Galan, 2000), and since these regions have been removed during structure determination of their corresponding GAP domains, they may already exist in a partially unfolded conformation prior to chaperone binding. However, based on our structure determination, there is no region of this size in AvrPphF ORF2 which is not folded into the structure described previously. We have been able to demonstrate interaction of AvrPphF ORF1 and ORF2 in vitro (data not shown) and can isolate such complexes on gel filtration columns. Structure determination of these complexes will allow us to answer unresolved questions about the mechanism of interaction of this chaperone-effector pair.

The structure of the type III effector AvrPphF ORF2 forms a new fold that structurally resembles a mushroom and can be subdivided into head and stalk subdomains. The stalk subdomain does not share significant structural similarity to known structures, whereas the head subdomain shares structural similarity to the catalytic domain of various ADP-RT toxins. However, we did not detect any ADP-RT activity, NAD binding, or NAD glycohydrolase activity associated with AvrPphF ORF2. Additionally, function could not be assigned using sequence-based searches such as PSI-BLAST, various threading algorithms (e.g., 3D-PSSM [Kelley et al., 2000]), or the direct three-dimensional comparison of protein folds (e.g., DALI) or spatial patterns of residues (i.e., PINTS [Stark et al., 2003]). It remains possible that AvrPphF ORF2 acts by binding and not by catalysis.

Despite the lack of ADP-RT activity, we used the structural similarity between AvrPphF ORF2 and diphtheria toxin to predict amino acids important for the virulence activity of AvrPphF ORF2. We experimentally confirmed these predictions for two of these residues, Arg72 and Asp174. In addition, when these mutant proteins were purified upon expression in *E. coli*, they were soluble, monomeric, and had circular dichroism spectra identical to wild-type protein, indicating that these mutations did not affect the solubility, aggregation state, or folding of AvrPphF ORF2.

Another structurally based criterion that was successful in predicting residues important for virulence activity was the identification of clusters of conserved amino acids with exposed side chains. Residues conserved among the AvrPphF ORF2 alleles clustered in two large cavities on the effector, which we identified as pocket A and pocket B. These two conserved regions are located on opposite sides of the molecule and possess different characteristics. Pocket A is located in the "head" of the protein and forms part of a groove running down the length of the molecule. Pocket B is less depressed than pocket A and lies at the interface between the head and the stalk subdomains. Based on mutational data, both surfaces are necessary for virulence facilitated by AvrPphF ORF2 as well as its ability to trigger host disease resistance mediated by the bean *R1* gene. The mutations are beyond the first 60 amino acids of the N terminus typically required for type III effector translocation by plant and animal pathogens, and are therefore unlikely to affect delivery by the type III secretion system (Anderson et al., 1999; Mudgett et al., 2000; Page and Parsot, 2002). Similarly, previous mutagenesis studies of the type III effector AvrPto revealed that out of 21 point mutations, only one affected translocation (Chang et al., 2001). Furthermore, this mutation resulted in an amino acid change from a histidine to a proline, a mutation that could potentially have deleterious structural effects (Chang et al., 2001).

The virulence function of type III effectors is thought to result from their activity on one or more host targets, altering host cell defense or physiology to favor survival of the pathogen. Correspondingly, mutations that disrupt a type III effector's ability to trigger specific plant immune response should also disrupt virulence function. This mechanistic scenario also posits that the result of the type III effector's virulence activity is the signal for specific plant disease resistance gene function (Dangl and Jones, 2001; Van der Biezen and Jones, 1998). Several recent studies support this hypothesis. Mutating the catalytic triad of the cysteine protease type III effector AvrPphB abolishes the hypersensitive response in resistant plant cultivars (Shao et al., 2002). Likewise, catalytic triad mutants of the predicted cysteine protease AvrRpt2 compromise its ability to elicit *RPS2*-dependent defense responses (Axtell et al., 2003). In accordance with this model, we observed that mutations decreasing the virulence of AvrPphF ORF2 on a susceptible cultivar (Tendergreen) also allowed *P. syringae* to grow better on a resistant cultivar (Red Mexican) (Figure 6), presumably by evading an immune response dependent on the virulence function of AvrPphF ORF2. However, the biochemical function of AvrPphF ORF2 remains elusive.

Part of the problem in assigning function from the structure of virulence factors is that pathogenic bacteria have evolved proteins that interact with eukaryotic tar-

gets, and in doing so they may have generated folds which differ considerably from their mammalian functional counterparts. As an example, *Salmonella* sp. produce a type III effector, SopE, that acts as an exchange factor for mammalian Rho family GTPases. The SopE fold is very different from the metazoan Dbl homology domain serving the same function (Buchwald et al., 2002).

Overall, our results demonstrate that functionally important domains of type III effectors with unknown enzymatic function can be predicted from their three-dimensional structure. The novelty of the AvrPphF ORF2 structure predicts that the outcome of a large-scale structural study of type III effectors from *P. syringae* will likely reveal many novel structures adopted to interact with eukaryotic host targets. However, as demonstrated by our structure-based functional analyses of AvrPphF ORF2 and the recently published crystal structure of the *Pseudomonas syringae* effector AvrB (Lee et al., 2004), the novelty of effector folds may also pose challenges for attribution of biochemical functions to these proteins.

## Experimental Procedures

### Cloning of AvrPphF ORF1 and ORF2

For bacterial expression as N-terminally histidine-tagged proteins, AvrPphF ORF1 and AvrPphF ORF2 were amplified by PCR from *Pph* race 7 cells and cloned into pProEX-HTa (Invitrogen) digested with NcoI and EcoRI. To add an N-terminal GST tag, AvrPphF ORF2 was amplified by PCR using oligonucleotides that incorporated an N-terminal TEV cleavage site and subcloned into pENTR D-TOPO vector (Invitrogen). The gene was then recombined into pDEST-15 vector using the LR Clonase enzyme mix according to manufacturer's instructions (Invitrogen). For AvrPphF ORF1, the sequence of two independent clones indicated an insertion of a single adenine at position 369 relative to its NCBI database entry (AF231453). This insertion alters and shortens the C-terminal amino acid sequence to VKKTFGFV from the reported VKKRLDLSESSV. The observed insertion of adenine was confirmed in the sequences of two independent PCR products generated using a proofreading enzyme. These data strongly indicated that the original sequence of AvrPphF ORF1 as deposited carries a sequencing error. For AvrPphF ORF2 cloning, the reverse PCR primer incorporated an in-frame HA-epitope coding sequence onto the C-terminal end of *avrPphF*, followed by a stop codon and a BamHI site. The resulting PCR product was cloned into Topo pCR2.1 (Invitrogen) and sequenced. For AvrPphF ORF2, the sequence of two independent clones was identical to its NCBI database entry (AF231453). The AvrPphF-HA construct was then cloned as an XbaI-BamHI fragment into the pDSK600 vector.

### Protein Expression and Purification

AvrPphF ORF1 and ORF2 in pProEX-HTa were induced with 0.75 mM IPTG at 18°C for 10 hr in *E. coli* BL21 Codon Plus RIL cells (Stratagene). For selenomethionine substitution, protein expression was induced in the methionine auxotrophic *E. coli* strain B831 DE3 (Novagen) grown in 2 liters of minimal medium containing 100 mg $l^{-1}$ selenomethionine (Acros). Protein purification of AvrPphF ORF1 and AvrPphF ORF2 followed similar protocols. Cell pellets were resuspended in buffer A (20 mM sodium phosphate [pH 7.5], 10 mM imidazole, 150 mM NaCl, and 10% glycerol) and lysed using an Avestin Emulsiflex-C5, and clarified lysates were added to 5 ml High Trap chelating columns (Amersham Biosciences) preloaded with nickel according to the manufacturer's instructions. Columns were washed with several volumes of buffer A augmented with 10–50 mM imidazole followed by specific elution of the histidine-tagged proteins with buffer A plus 400 mM imidazole. AvrPphF ORF2 proteins (wild-type and mutant) were also expressed in *E. coli* and isolated as GST fusion proteins with a TEV cleavage site between the GST and cloned protein. Cell pellets in this case were resuspended in a buffer containing 20 mM HEPES (pH 7.5), 50 mM NaCl, and 1 mM DTT, lysed and clarified as before, and added to a 5 ml High Trap glutathione column (Amersham Biosciences). The column was then washed with 10 column volumes of buffer, followed by 5 column volumes of this buffer plus 10 mM glutathione to elute the protein. N-terminal histidine and GST tags were removed by the addition of TEV (tobacco etch virus) protease produced and purified in-house while dialyzing the proteins overnight in low-salt buffer containing 20 mM Tris (pH 8.0). Following confirmation of complete removal of all tags by SDS-PAGE, dialysates were loaded onto an 8 ml Source S (Amersham Biosciences) cation exchange column and eluted with a gradient of NaCl. Appropriate fractions were subsequently applied to a HighPrep 26/20 Sephacryl S200 (Pharmacia) column equilibrated with 20 mM HEPES (pH 7.5), 150 mM NaCl. This last step provided minimal increases in protein purity and confirmed the dimeric and monomeric nature of AvrPphF ORF1 and ORF2, respectively. This column was also used to confirm the mobility of mutant AvrPphF ORF2 proteins as shown in Figure 6D. Purified protein was concentrated to 10–12 mg $ml^{-1}$, flash-frozen using liquid $N_2$, and stored at −80°C. AvrPphF ORF2 purified using either initially His-tagged or GST-tagged systems was found to be folded identically by circular dichroism (data not shown; see below).

Circular dichroism experiments were run on a Pistar-180 Circular Dichroism/Fluorescence spectrometer (Applied Photophysics). Samples (with protein concentrations between 0.07 and 0.21 mg/ml) were placed in a 0.1 cm cuvette, and scans were taken from 185 to 260 nm with 0.2 nm increments and 30,000 repetitions per increment.

### Crystallization

Conditions for crystallization of AvrPphF ORF1 and AvrPphF ORF2 were found by screening on 96-well plates using a Gilson C-240 workstation and commercially available (Hampton Research; Emerald Biostructures) and hand-made screens. Final conditions for the crystallization of AvrPphF ORF1 were obtained by vapor diffusion of a 1:1 mix of protein (12 mg/ml) with well solution (80 mM Tris [pH 7.5] and 1.4–2.0 M $(NH_4)_2SO_4$) at 4°C. Single crystals grew in 3–5 days and had a modified tetrahedral morphology ~200–400 μm in length. Crystals were orthorhombic ($P2_12_12_1$, a = 93.1 Å, b = 94.9 Å, and c = 104.4 Å) and could be cryoprotected by soaking in well solution containing 25% v/v glycerol for short periods of time (30 s or less).

Crystals of AvrPphF ORF2 were also grown using vapor diffusion of a 1:1 mixture of protein (10 mg/ml) with well solution. However, two different conditions (well solutions) could be used, namely 16% PEG8000, 150 mM Mg acetate, 80 mM Bis-Tris (pH 6.5), and 15% glycerol, and 1.5 M $(NH_4)_2SO_4$, 2% PEG400, 80 mM HEPES (pH 7.5), and 20% glycerol. Crystals grown under either condition were orthorhombic ($P2_12_12_1$) with similar cell dimensions (see below), diffracted to as high as 2 Å resolution, and were of similar quality. Both crystallization conditions are inherently cryoprotective.

### Structure Determination

For AvrPphF ORF1, diffraction data were collected at the SER-CAT beamline (ID-22; Advanced Photon Source) using a single crystal containing selenomethionine-substituted protein (Doublie, 1997). Phases were determined using MAD. The program SOLVE (Terwilliger and Berendzen, 1999) was used to find 12 selenium atoms in the asymmetric unit (3 per monomer, 2 chaperone dimers per asymmetric unit). Solvent-flattened maps calculated by DM (CCP4, 1994) were traced for one monomer using the program O (Jones and Kjeldgaard, 1997) followed by the application of noncrystallographic symmetry to place the remaining monomers. Refinement was carried out with CNS while applying restrained 4-fold noncrystallographic symmetry (Brunger et al., 1998). In the final model, the final 2 residues are missing in all four molecules. The final model contains 4276 atoms, including 1 sulfate ion per monomer and a Gly-Ala dipeptide cloning artifact at the N terminus of each monomer. Due to the low resolution, no water molecules were included in the model (see Table 1 for X-ray data collection and refinement statistics).

For AvrPphF ORF2, data were collected on a Rigaku RU-H3R rotating anode generator equipped with Osmic confocal "blue" optics, and diffraction intensities were recorded on an R-Axis IV++ image plate system. The structure was solved by the solvent heavy-

atom method (using cesium) of MIRAS (Dauter et al., 2000, 2001). The crystallization medium was already competent to be a cryosolvent; crystals from the PEG8000 conditions (see above, with cell dimensions a = 38.7 Å, b = 68.3 Å, c = 88.4 Å) were subsequently soaked for 30 s in 0.8 M CsCl plus crystallization mother liquor. The SHELXD program (Schneider and Sheldrick, 2002) was used to find 14 unique Cs atoms. The SHELXE program was used to choose the correct hand of the heavy-atom positions and to prepare solvent-flattened maps with the experimental MIRAS phases, which were extended to 2.0 Å using diffraction data from a crystal from the PEG 8000 conditions not soaked in CsCl (native data set). The experimental maps were of sufficient quality to trace rapidly 176 of the 210 amino acids in the expressed sequence using the program O (Jones and Kjeldgaard, 1997). Subsequent refinement was carried out by CNS (Brunger et al., 1998) using rigid-body refinement followed by iterative rounds of simulated annealing torsion angle and B factor refinement. There are 1416 atoms in the final model, including 145 waters. Disordered regions not modeled include the N-terminal 28 residues and two loops (amino acids 147–153 and 177–180). Similarly, there was no observable electron density for the side chain of His126, so this residue has been modeled as an Ala. MOLPROBITY (Lovell et al., 2003) was also briefly used to correctly position His and Gln residues, as well as remove some bad contacts (see Table 1 for X-ray data collection and refinement statistics).

Ribbon diagrams were produced with MOLSCRIPT (Kraulis, 1991), secondary structure was calculated using DSSP (Kabsch and Sander, 1983), lipophilic surface potential was generated with SYBYL version 6.9.1 (www.tripos.com), other protein surfaces were rendered with GRASP (Nicholls et al., 1991), and buried surface areas were calculated with NACCESS (Hubbard and Thornton, 1993). Multiple-sequence alignments were produced with ClustalX (Jeanmougin et al., 1998) or DALI (Holm and Sander, 1993) when guided by three-dimensional structures.

### In Planta Growth Assays

AvrPphF ORF1 was amplified from *P. syringae* pv. *phaseolicola* (*Pph*) race 7 (Tsiamis et al., 2000) and cloned into the broad host-range plasmid pBBR1 MCS-2 under control of the *lacZ/npt2* promoter. AvrPphF ORF2 was also amplified from *Pph* race 7 and cloned into the pDSK 600 plasmid. The various AvrPphF ORF2 mutations were made by PCR and also cloned into pDSK 600. All constructs were transformed into the *Pph* strain RW60, which is cured of the plasmid pAV511 that normally harbors *avrPphF* ORF1 and ORF2 (Jackson et al., 1999). Bacterial cultures were grown overnight in KB media containing appropriate antibiotics. Bacteria were resuspended in 10 mM $MgCl_2$ to $OD_{600}$ = 0.1 ($\sim 5 \times 10^7$) and diluted to $1 \times 10^6$ for growth curves. Three-week-old Tendergreen or Red Mexican bean cultivars were hand inoculated with appropriate bacterial strains using a 3 ml syringe. Bacterial multiplication was measured as described previously (Tsiamis et al., 2000).

For Western blot analysis, 2.5 ml overnight cultures grown in KB media with appropriate antibiotics were spun down and resuspended in 500 μl of 1× Laemmli buffer. Samples were boiled 5 min, and 10 μl was loaded on an SDS-PAGE gel. Immunodetection was performed by standard methods.

### Acknowledgments

We thank Prof. John Mansfield, Wye College, UK, for bacterial strains, Dr. A. Rod Merrill for his *P. aeruginosa* exotoxin-A expressing *E. coli*, and Nadia Leyarovska at the 22-ID beamline (SER-CAT) at the Advanced Photon Source, Argonne National Laboratory, for help in data collection. This work was supported by grants from the United States Department of Energy (DEFG05-95ER20187) to J.L.D. and the NIH (GM-65533) to J.S. D.D. is a fellow of the Natural Science and Engineering Research Council (NSERC) of Canada, and J.H.C. was supported by an NIH-NRSA Fellowship (F32-GM20296-02S1).

Received: April 20, 2004
Revised: June 17, 2004
Accepted: June 24, 2004
Published: September 7, 2004

### References

Anderson, D.M., Fouts, D.E., Collmer, A., and Schneewind, O. (1999). Reciprocal secretion of proteins by the bacterial type III machines of plant and animal pathogens suggests universal recognition of mRNA targeting signals. Proc. Natl. Acad. Sci. USA *96*, 12839–12843.

Axtell, M.J., and Staskawicz, B.J. (2003). Initiation of RPS2-specified disease resistance in *Arabidopsis* is coupled to the AvrRpt2-directed elimination of RIN4. Cell *112*, 369–377.

Axtell, M., Chisholm, S., Dahlbeck, D., and Staskawicz, B. (2003). Genetic and molecular evidence that the *Pseudomonas syringae* type III effector protein AvrRpt2 is a cysteine protease. Mol. Microbiol. *49*, 1537–1546.

Beattie, B., and Merrill, A. (1999). A fluorescence investigation of the active site of *Pseudomonas aeruginosa* exotoxin A. J. Biol. Chem. *274*, 15646–15654.

Bennett, M.J., Choe, S., and Eisenberg, D. (1994). Refined structure of dimeric diphtheria toxin at 2.0 Å resolution. Protein Sci. *3*, 1444–1463.

Birtalan, S., and Ghosh, P. (2001). Structure of the *Yersinia* type III secretory system chaperone SycE. Nat. Struct. Biol. *8*, 974–978.

Birtalan, S.C., Phillips, R.M., and Ghosh, P. (2002). Three-dimensional secretion signals in chaperone-effector complexes of bacterial pathogens. Mol. Cell *9*, 971–980.

Boch, J., Joardar, V., Gao, L., Robertson, T.L., Lim, M., and Kunkel, B.N. (2002). Identification of Pseudomonas syringae pv. tomato genes induced during infection of Arabidopsis thaliana. Mol. Microbiol. *44*, 73–88.

Brunger, A.T., Adams, P.D., Clore, G.M., DeLano, W.L., Gros, P., Grosse-Kunstleve, R.W., Jiang, J.S., Kuszewski, J., Nilges, M., Pannu, N.S., et al. (1998). Crystallography & NMR system: a new software suite for macromolecular structure determination. Acta Crystallogr. D Biol. Crystallogr. *54*, 905–921.

Buchwald, G., Friebel, A., Galan, J., Hardt, W., Wittinghofer, A., and Scheffzek, K. (2002). Structural basis for the reversible activation of a Rho protein by the bacterial toxin SopE. EMBO J. *21*, 3288–3295.

CCP4 (Collaborative Computational Project, Number 4) (1994). The CCP4 suite: programs for protein crystallography. Acta Crystallogr. D Biol. Crystallogr. *50*, 760–763.

Chang, J.H., Rathjen, J.P., Bernal, A.J., Staskawicz, B.J., and Michelmore, R.W. (2000). avrPto enhances growth and necrosis caused by *Pseudomonas syringae* pv. *tomato* in tomato lines lacking either Pto or Prf. Mol. Plant Microbe Interact. *13*, 568–571.

Chang, J.H., Tobias, C.M., Staskawicz, B.J., and Michelmore, R.W. (2001). Functional studies of the bacterial avirulence protein AvrPto by mutational analysis. Mol. Plant Microbe Interact. *14*, 451–459.

Chen, Z., Kloek, A.P., Boch, J., Katagiri, F., and Kunkel, B.N. (2000). The *Pseudomonas syringae* avrRpt2 gene product promotes pathogen virulence from inside plant cells. Mol. Plant Microbe Interact. *13*, 1312–1321.

Coburn, J., Wyatt, R.T., Iglewski, B.H., and Gill, D.M. (1989). Several GTP-binding proteins, including p21c-H-ras, are preferred substrates of *Pseudomonas aeruginosa* exoenzyme S. J. Biol. Chem. *264*, 9004–9008.

Collmer, A., Lindeberg, M., Petnicki-Ocwieja, T., Schneider, D.J., and Alfano, J.R. (2002). Genomic mining type III secretion system effectors in *Pseudomonas syringae* yields new picks for all TTSS prospectors. Trends Microbiol. *10*, 462–469.

Cornelis, G.R. (2002). The *Yersinia* Ysc-Yop 'type III' weaponry. Mol. Cell. Biol. *3*, 742–754.

Dangl, J.L., and Jones, J.D. (2001). Plant pathogens and integrated defence responses to infection. Nature *411*, 826–833.

Dauter, Z., Dauter, M., and Rajashankar, K.R. (2000). Novel approach to phasing proteins: derivatization by short cryo-soaking with halides. Acta Crystallogr. D Biol. Crystallogr. *56*, 232–237.

Dauter, Z., Li, M., and Wlodawer, A. (2001). Practical experience with the use of halides for phasing macromolecular structures: a

powerful tool for structural genomics. Acta Crystallogr. D Biol. Crystallogr. *57*, 239–249.

Doublie, S. (1997). Preparation of selenomethionyl proteins for phase determination. In Methods in Enzymology, C.W. Carter and R.W. Sweet, eds. (San Diego, CA: Academic Press), pp. 523–530.

Espinosa, A., Guo, M., Tam, V.C., Fu, Z.Q., and Alfano, J.R. (2003). The *Pseudomonas syringae* type III-secreted protein HopPtoD2 possesses protein tyrosine phosphatase activity and suppresses programmed cell death in plants. Mol. Microbiol. *49*, 377–387.

Evdokimov, A.G., Tropea, J.E., Routzahn, K.M., and Waugh, D.S. (2002). Three-dimensional structure of the type III secretion chaperone SycE from *Yersinia pestis*. Acta Crystallogr. D Biol. Crystallogr. *58*, 398–406.

Fouts, D.E., Abramovitch, R.B., Alfano, J.R., Baldo, A.M., Buell, C.R., Cartinhour, S., Chatterjee, A.K., D'Ascenzo, M., Gwinn, M.L., Lazarowitz, S.G., et al. (2002). Genomewide identification of *Pseudomonas syringae* pv. *tomato* DC3000 promoters controlled by the HrpL alternative sigma factor. Proc. Natl. Acad. Sci. USA *99*, 2275–2280.

Galan, J.E. (2001). *Salmonella* interactions with host cells: type III secretion at work. Annu. Rev. Cell Dev. Biol. *17*, 53–86.

Gauthier, A., and Finlay, B.B. (2003). Translocated intimin receptor and its chaperone interact with ATPase of the type III secretion apparatus of enteropathogenic *Escherichia coli*. J. Bacteriol. *185*, 6746–6755.

Ghose, A., Viswanadhan, V., and Wendoloski, J. (1998). Prediction of hydrophobic (lipophilic) properties of small organic molecules using fragmental methods: an analysis of ALOGP and CLOGP methods. J. Phys. Chem. A *102*, 3762–3772.

Greenberg, J.T., and Vinatzer, B.A. (2003). Identifying type III effectors of plant pathogens and analyzing their interaction with plant cells. Curr. Opin. Microbiol. *6*, 20–28.

Guttman, D.S., Vinatzer, B.A., Sarkar, S.F., Ranall, M.V., Kettler, G., and Greenberg, J.T. (2002). A functional screen for the type III (Hrp) secretome of the plant pathogen *Pseudomonas syringae*. Science *295*, 1722–1726.

Hansen-Wester, I., and Hensel, M. (2001). *Salmonella* pathogenicity islands encoding type III secretion systems. Microbes Infect. *3*, 549–559.

Holm, L., and Sander, C. (1993). Protein structure comparison by alignment of distance matrices. J. Mol. Biol. *233*, 123–138.

Hubbard, S.J., and Thornton, J.M. (1993). NACCESS, 2.1.1 Edition (computer program). Department of Biochemistry and Molecular Biology, University College, London.

Iglewski, B.H., and Kabat, D. (1975). NAD-dependent inhibition of protein synthesis by *Pseudomonas aeruginosa* toxin. Proc. Natl. Acad. Sci. USA *72*, 2284–2288.

Jackson, R.W., Athanassopoulos, E., Tsiamis, G., Mansfield, J.W., Sesma, A., Arnold, D.L., Gibbon, M.J., Murillo, J., Taylor, J.D., and Vivian, A. (1999). Identification of a pathogenicity island, which contains genes for virulence and avirulence, on a large native plasmid in the bean pathogen *Pseudomonas syringae* pathovar phaseolicola. Proc. Natl. Acad. Sci. USA *96*, 10875–10880.

Jeanmougin, F., Thompson, J.D., Gouy, M., Higgins, D.G., and Gibson, T.J. (1998). Multiple sequence alignment with Clustal X. Trends Biochem. Sci. *23*, 403–405.

Jin, Q., Thilmony, R., Zwiesler-Vollick, J., and He, S.Y. (2003). Type III protein secretion in *Pseudomonas syringae*. Microbes Infect. *5*, 301–310.

Jones, T., and Kjeldgaard, M. (1997). Electron-density map interpretation. In Methods in Enzymology, C.W. Carter and R.W. Sweet, ed. (San Diego, CA: Academic Press). 173–208.

Kabsch, W., and Sander, C. (1983). Dictionary of protein secondary structure: pattern recognition of hydrogen-bonded and geometrical features. Biopolymers *22*, 2577–2637.

Keen, N.T., Tamaki, S., Kobayashi, D., and Trollinger, D. (1988). Improved broad-host-range plasmids for DNA cloning in gram-negative bacteria. Gene *70*, 191–197.

Kelley, L.A., MacCallum, R.M., and Sternberg, M.J. (2000). Enhanced genome annotation using structural profiles in the program 3D-PSSM. J. Mol. Biol. *299*, 499–520.

Kovach, M.E., Elzer, P.H., Hill, D.S., Robertson, G.T., Farris, M.A., Roop, R.M., 2nd, and Peterson, K.M. (1995). Four new derivatives of the broad-host-range cloning vector pBBR1MCS, carrying different antibiotic-resistance cassettes. Gene *166*, 175–176.

Kraulis, P. (1991). MOLSCRIPT: a program to produce both detailed and schematic plots of protein structures. Acta. Crystallogr. D Biol. Crystallogr. *24*, 946–950.

Lee, C.C., Wood, M.D., Ng, K., Andersen, C.B., Liu, Y., Luginbuhl, P., Spraggon, G., and Katagiri, F. (2004). Crystal structure of the type III effector AvrB from *Pseudomonas syringae*. Structure *12*, 487–494.

Lorang, J.M., and Keen, N.T. (1995). Characterization of avrE from *Pseudomonas syringae* pv. *tomato*: a hrp-linked avirulence locus consisting of at least two transcriptional units. Mol. Plant Microbe Interact. *8*, 49–57.

Lovell, S.C., Davis, I.W., Arendall, W.B., 3rd, de Bakker, P.I., Word, J.M., Prisant, M.G., Richardson, J.S., and Richardson, D.C. (2003). Structure validation by C$\alpha$ geometry: $\phi$,$\Psi$ and C$\beta$ deviation. Proteins *50*, 437–450.

Luo, Y., Bertero, M.G., Frey, E.A., Pfuetzner, R.A., Wenk, M.R., Creagh, L., Marcus, S.L., Lim, D., Sicheri, F., Kay, C., et al. (2001). Structural and biochemical characterization of the type III secretion chaperones CesT and SigE. Nat. Struct. Biol. *8*, 1031–1036.

Mackey, D., Holt, B.F., Wiig, A., and Dangl, J.L. (2002). RIN4 interacts with *Pseudomonas syringae* type III effector molecules and is required for RPM1-mediated resistance in *Arabidopsis*. Cell *108*, 743–754.

Mackey, D., Belkhadir, Y., Alonso, J.M., Ecker, J.R., and Dangl, J.L. (2003). *Arabidopsis* RIN4 is a target of the type III virulence effector AvrRpt2 and modulates RPS2-mediated resistance. Cell *112*, 379–389.

Makarova, K.S., Aravind, L., and Koonin, E.V. (1999). A superfamily of archaeal, bacterial, and eukaryotic proteins homologous to animal transglutaminases. Protein Sci. *8*, 1714–1719.

Mudgett, M.B., Chesnokova, O., Dahlbeck, D., Clark, E.T., Rossier, O., Bonas, U., and Staskawicz, B.J. (2000). Molecular signals required for type III secretion and translocation of the *Xanthomonas campestris* AvrBs2 protein to pepper plants. Proc. Natl. Acad. Sci. USA *97*, 13324–13329.

Nicholls, A., Sharp, K.A., and Honig, B. (1991). Protein folding and association: insights from the interfacial and thermodynamic properties of hydrocarbons. Proteins *11*, 281–296.

Nimchuk, Z., Rohmer, L., Chang, J.H., and Dangl, J.L. (2001). Knowing the dancer from the dance: R-gene products and their interactions with other proteins from host and pathogen. Curr. Opin. Plant Biol. *4*, 288–294.

Page, A.L., and Parsot, C. (2002). Chaperones of the type III secretion pathway: jacks of all trades. Mol. Microbiol. *46*, 1–11.

Parsot, C., Hamiaux, C., and Page, A.L. (2003). The various and varying roles of specific chaperones in type III secretion systems. Curr. Opin. Microbiol. *6*, 7–14.

Petnicki-Ocwieja, T., Schneider, D.J., Tam, V.C., Chancey, S.T., Shan, L., Jamir, Y., Schechter, L.M., Janes, M.D., Buell, C.R., Tang, X., et al. (2002). Genomewide identification of proteins secreted by the Hrp type III protein secretion system of *Pseudomonas syringae* pv. *tomato* DC3000. Proc. Natl. Acad. Sci. USA *99*, 7652–7657.

Provencher, S., and Glockner, J. (1981). Estimation of globular protein secondary structure from circular dichroism. Biochemistry *20*, 33–37.

Ritter, C., and Dangl, J.L. (1995). The avrRpm1 gene of *Pseudomonas syringae* pv. *maculicola* is required for virulence on Arabidopsis. Mol. Plant Microbe Interact. *8*, 444–453.

Schneider, T.R., and Sheldrick, G.M. (2002). Substructure solution with SHELXD. Acta Crystallogr. D Biol. Crystallogr. *58*, 1772–1779.

Shan, L., Oh, H., Chen, J., Guo, M., Zhou, J., Alfano, J.R., Collmer, A., Jia, X., and Tang, X. (2004). The *HopPtoF* Locus of *Pseudomonas*

*syringae* pv. DC3000 encodes a type III chaperone and a cognate effector. Mol. Plant Microbe Interact. *17*, 447–455.

Shao, F., Merritt, P.M., Bao, Z., Innes, R.W., and Dixon, J.E. (2002). A *Yersinia* effector and a *Pseudomonas* avirulence protein define a family of cysteine proteases functioning in bacterial pathogenesis. Cell *109*, 575–588.

Shao, F., Golstein, C., Ade, J., Stoutemyer, M., Dixon, J.E., and Innes, R.W. (2003). Cleavage of *Arabidopsis* PBS1 by a bacterial type III effector. Science *301*, 1230–1233.

Stark, A., Sunyaev, S., and Russell, R.B. (2003). A model for statistical significance of local similarities in structure. J. Mol. Biol. *326*, 1307–1316.

Staskawicz, B.J., Mudgett, M.B., Dangl, J.L., and Galan, J.E. (2001). Common and contrasting themes of plant and animal diseases. Science *292*, 2285–2289.

Stebbins, C.E., and Galan, J.E. (2000). Modulation of host signaling by a bacterial mimic: structure of the *Salmonella* effector SptP bound to Rac1. Mol. Cell *6*, 1449–1460.

Stebbins, C.E., and Galan, J.E. (2001). Maintenance of an unfolded polypeptide by a cognate chaperone in bacterial type III secretion. Nature *414*, 77–81.

Takada, T., Iida, K., and Moss, J. (1995). Conservation of a common motif in enzymes catalyzing ADP-ribose transfer. Identification of domains in mammalian transferases. J. Biol. Chem. *270*, 541–544.

Terwilliger, T.C., and Berendzen, J. (1999). Automated MAD and MIR structure solution. Acta Crystallogr. D Biol. Crystallogr. *55*, 849–861.

Tsiamis, G., Mansfield, J.W., Hockenhull, R., Jackson, R.W., Sesma, A., Athanassopoulos, E., Bennett, M.A., Stevens, C., Vivian, A., Taylor, J.D., and Murillo, J. (2000). Cultivar-specific avirulence and virulence functions assigned to avrPphF in *Pseudomonas syringae* pv. *phaseolicola*, the cause of bean halo-blight disease. EMBO J. *19*, 3204–3214.

Van der Biezen, E.A., and Jones, J.D. (1998). Plant disease-resistance proteins and the gene-for-gene concept. Trends Biochem. Sci. *23*, 454–456.

Van der Hoorn, R.A., De Wit, P.J., and Joosten, M.H. (2002). Balancing selection favors guarding resistance proteins. Trends Plant Sci. *7*, 67–71.

Viswandam, V., Ghose, A., Revankar, G., and Robins, R. (1989). Atomic physicochemical parameters for three dimensional structure directed quantitative structure-activity relationships. 4. Additional parameters for hydrophobic and dispersive interactions and their application for an automated superposition of certain naturally occurring nucleoside antibiotics. J. Chem. Inf. Comput. Sci. *29*, 163–172.

Zwiesler-Vollick, J., Plovanich-Jones, A.E., Nomura, K., Bandyopadhyay, S., Joardar, V., Kunkel, B.N., and He, S.Y. (2002). Identification of novel hrp-regulated genes through functional genomic analysis of the *Pseudomonas syringae* pv. *tomat*o DC3000 genome. Mol. Microbiol. *45*, 1207–1218.

## Accession Numbers

AvrPphF ORF1 and ORF2 have been deposited in the Protein Data Bank with accession codes 1S28 and 1S21, respectively.

## Note Added in Proof

A unification of nomenclature for type III effector proteins and their chaperones has recently been defined (M. Lindeberg et. al., submitted). AvrPphF and related proteins from various *P. syringae* pathovars are members of the newly designated HopF2 family, and the AvrPphF ORF1 chaperone will be termed ShcF.